Physics Mechanisms of Toroidal Rotation Profile and Properties of Momentum Transport in JT-60U

Maiko YOSHIDA, Yutaka KAMADA, Hidenobu TAKENAGA, Yoshiteru SAKAMOTO, Hajime URANO, Naoyuki OYAMA, Go MATSUNAGA and the JT-60 Team

Japan Atomic Energy Agency, 801-1, Mukoyama, Naka 311-0193, Japan

(Received 29 November 2007 / Accepted 3 March 2008)

The roles of momentum transport on the toroidal rotation velocity (V_t) profile and the properties of transport coefficients are found by transient momentum transport analysis. The perturbation technique enables us to evaluate the momentum diffusivity (χ_ϕ) and the convection velocity (V_{conv}), and to calculate V_t profiles driven by external torque input by neutral beams (*NBs*). The measured V_t profiles with and without the external torque input are almost reproduced by χ_ϕ and V_{conv} in low-β ($\beta_N < 0.4$) plasmas. At higher β, the local pressure gradient plays a role in determining the local value of intrinsic rotation velocity. Concerning the momentum transport, χ_ϕ increases with increasing heating power, and decreases with increasing plasma current (I_p). In H-mode plasmas, χ_ϕ is smaller than that in L-mode plasmas under similar experimental conditions. It is found that χ_ϕ, which is separated from the non-diffusive term increases with increasing heat diffusivity (χ_i), $\chi_\phi/\chi_i \sim$ 1-3, and $-V_{conv}$ increases with increasing χ_ϕ, $V_{conv}/\chi_\phi \sim -2.5$ to $-0.7\,\mathrm{m}^{-1}$, in H-mode plasmas.

Keywords: toroidal rotation velocity, momentum transport, L-mode, H-mode

DOI: 10.1585/pfr.3.S1007

1. Introduction

A burning plasma is a self-regulating system where the pressure, rotation, and current profiles are strongly linked to each other [1]. The JT-60 project has addressed major physics issues toward the understanding and operation of burning steady-state plasmas, and promoted an integrated research project focusing on the rotation. Momentum transport is one of the crucial parameters for determination of the rotation profile. Therefore, it is of critical importance in understanding the properties of momentum transport coefficients for prediction of the rotation in next step devices [2].

It is now widely recognized that rotation and its radial shear play essential roles in determining magnetohydrodynamic (MHD) stability at a high plasma pressure, such as the stabilization of the resistive-wall mode [3–5], and in suppression of turbulence leading to enhanced confinement, such as transport barrier formation [6–8]. However, the mechanism determining the toroidal rotation velocity (V_t) profile is not understood well, because the V_t profiles are determined by various mechanisms, as shown in Fig. 1. The worldwide progress in understanding the physics of momentum transport and rotation has been made both experimentally [9–20] and theoretically [21–25]. As for the elements determining V_t, the characteristics of momentum transport, which consists of diffusive (toroidal momentum diffusivity, χ_ϕ) and non-diffusive (convection velocity, V_{conv}) terms [10,14,18], the external momentum input,

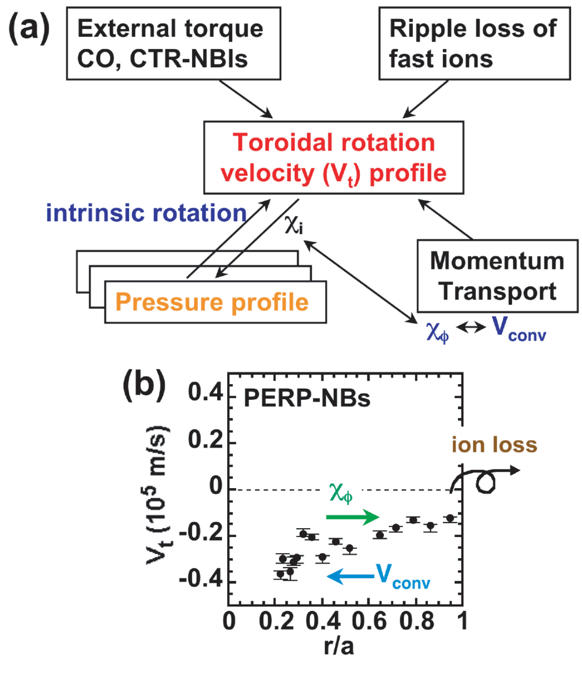

Fig. 1 (a) Approach to understanding the formation mechanism of the toroidal rotation (V_t) profile. (b) Example of $V_t(r)$ with only perpendicular NBs.

and the intrinsic rotation [15,17,19,23] have been reported individually. For example, concerning the toroidal momentum transport, most of the previous studies evaluated the diffusive term utilizing the steady-state momentum bal-

author's e-mail: yoshida.maiko@jaea.go.jp

ance equation, assuming that the momentum flux is diffusive [12]. However, the diffusive term is over- or underestimated when the non-diffusive term is not negligible, because the diffusive term evaluated by the steady-state momentum balance equation includes the non-diffusive terms. Non-diffusive terms in the toroidal momentum transport equation were evaluated by the analysis of the transport of toroidal rotation in the transient phase during tangential neutral beam (NB) injection [10, 11, 20], and that of the time evolution of V_t profiles [13]. The momentum pinch mechanism [24] and its dependences on various parameters are predicted [25] from theoretical models. However, the relations between χ_ϕ and heat diffusivity (χ_i), and χ_ϕ and V_{conv} after separating the diffusive and non-diffusive terms have not been understood experimentally. These correlations can contribute to the understanding of the anomalous momentum transport. In addition, the understanding of rotation mechanisms after integrating all of the elements shown in Fig. 1(a) remains an open issue despite its urgency toward the next step devices. This is due mainly to an experimental difficulty in evaluating the diffusive and non-diffusive terms of momentum transport separately.

In order to address this issue, we have applied the perturbation techniques developed in our recent studies [14, 18], which enable us to evaluate χ_ϕ and V_{conv} separately. As a novel momentum source, fast ion losses due to toroidal field ripple, which locally induce a toroidal rotation in the direction antiparallel to the plasma current, i.e., the counter (CTR) direction in the peripheral region, have been used [14]. An example of the V_t profile with only perpendicular NBs is shown in Fig. 1(b). As one can see, CTR-toroidal rotation is observed over the whole radius, and the CTR-toroidal rotation increases toward the core region despite a negligibly small torque input by NBs. For the explanation of this CTR-toroidal rotation, χ_ϕ, V_{conv}, and the boundary condition of V_t are needed. In Fig. 1(a), our approach to understanding the formation mechanism of the V_t profile is described.

This paper is arranged as follows. In section 2, the effects of the ripple loss of fast ions on the toroidal rotation are discussed using data with and without ferritic steel tiles (FSTs) [26]. The edge CTR rotation due to the ripple loss of fast ions is used as the edge-localized momentum source in the modulation experiments. Section 3 uses this momentum source in order to evaluate χ_ϕ and V_{conv} separately. In addition, the roles of these coefficients on V_t are identified in low-beta plasmas. Then, the formation mechanism of V_t profile in higher-beta, L- and H-mode plasmas is also presented with emphasis on the intrinsic rotation in section 3. The characteristics of χ_ϕ and V_{conv}, and the correlations between χ_ϕ, V_{conv}, and χ_i in L- and H-mode plasmas are discussed in sections 4 and 5. The comparison of χ_ϕ in L- and H-mode plasmas is also shown. Finally, a brief summary is given in section 6. In this paper, the negative sign of V_t designates CTR-directed rotation and the positive sign of V_t designates CO-directed rotation (with respect to the plasmas current), and the momentum balance equation is solved using a cylindrical model for toroidal momentum with flux surface-averaged parameters.

2. Driving Source of CTR Rotation

In JT-60U [27], NBs of various injection geometries are installed. They consist of two tangential beams directed along the same direction as that of the plasma current (CO-NBs), two tangential beams directed opposite to the plasma current (CTR-NBs), and seven near-perpendicular beams, as shown in Fig. 2(a). The injection angle of the tangential beams is 36 degrees and that of the near-perpendicular neutral beam (PERP-NB) is 75 degrees with respect to the magnetic axis. The deuterium beam acceleration energy is about 85 keV, and the input power per injected unit is about 2 MW. The plasma rotation in the

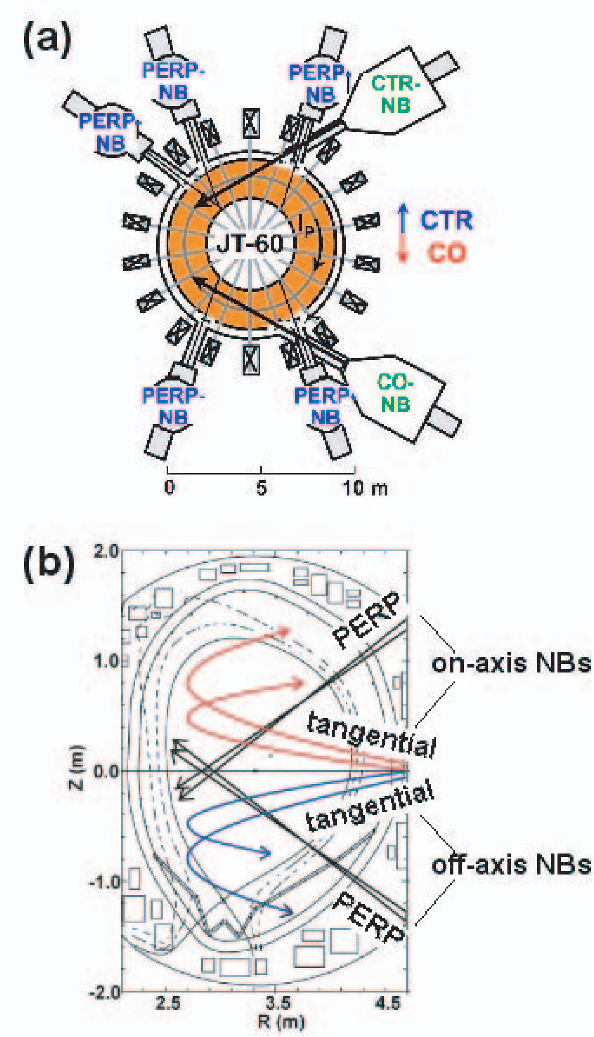

Fig. 2 (a) Neutral beam (NB) system on JT-60U (Top view). They consist of two CO-tangential beams, two CTR-tangential beams, and seven near-perpendicular beams (PERP-NBs). (b) Poloidal cross-section with NB trajectories. Neutral beams have two ion sources in each unit.

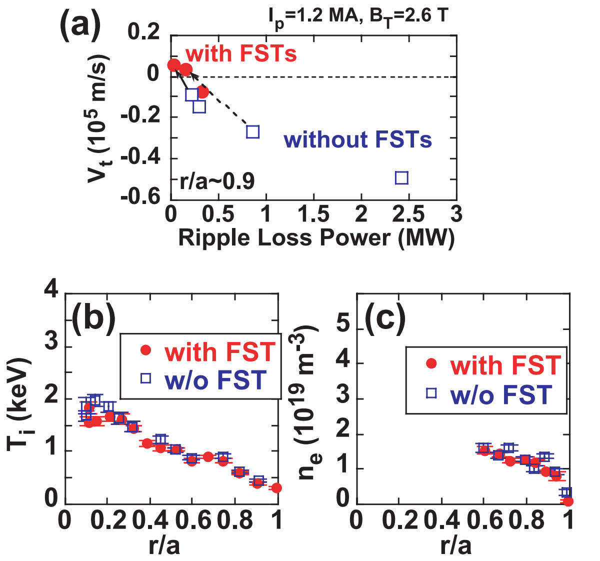

Fig. 3 (a) V_t dependence on the ripple loss power in the peripheral region evaluated using NB power and toroidal field ripple scans. Profiles of (b) ion temperature T_i, and (c) electron density n_e with and without FSTs in the L-mode with P_{ABS} ~ 1.4-1.8 MW (solid arrow in Fig. 3(a)).

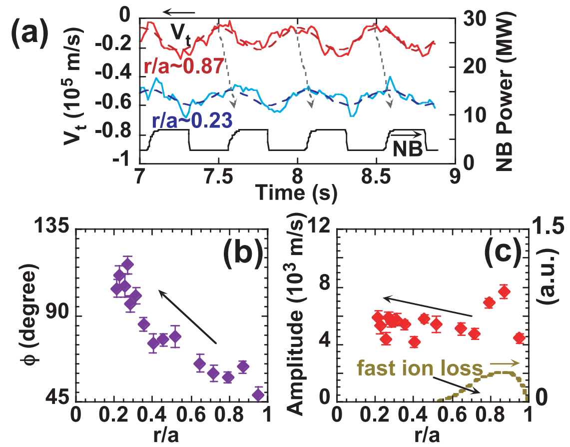

Fig. 4 (a) Response of V_t to modulated beams. Two traces of V_t at r/a ~ 0.87 and 0.23 are shown (I_P = 0.87 MA, B_T = 3.8 T, q_{95} = 8.2, *Vol.* = 72 m^3, L-mode). Each trace is fitted to a sinusoidal function using the modulation frequency (dotted lines). Profiles of (b) phase delay (ϕ), (c) modulated amplitude (V_{t0}), and prompt fast ion loss.

toroidal direction is varied using a combination of these NBs. In addition to such a direction, one of the two tangential beams in the same direction is used for almost on-axis deposition and the other for off-axis deposition, four of the PERP-NBs are used for almost on-axis deposition and the others for off-axis deposition, as shown in Fig. 2(b). In this paper, the main plasma parameters concerning the plasma configuration are the major radius R = 3.35-3.44 m, minor radius a = 0.87-0.95 m, triangularity at separatrix δ_x = 0.32-0.35, and elongation at separatrix κ_x = 1.33-1.39.

In JT-60U, CTR rotation is observed with PERP-NB injections in the case with the large ripple loss condition. In this section, the effects of the ripple loss of fast ions and the location of the driving source of CTR rotation are investigated. The relation between V_t in the peripheral region (r/a ~ 0.9) and ripple loss power is obtained using NB power and the toroidal field ripple (with and without FSTs) scans, as shown in Fig. 3(a). In this data set, the plasma current (I_P), toroidal magnetic field (B_T), safety factor at 95% flux surface (q_{95}), plasma volume (*Vol.*), and line-averaged electron density ($\bar{n}_e$) are kept almost constant (I_p = 1.15 MA, B_T = 2.6 T, q_{95} ~ 4.1, *Vol.* ~ 65 m^3, $\bar{n}_e$ ~ 1.5-2 × 10^{19} m^{-3}). For the plasma of *Vol.* ~ 65 m^3, the maximum ripple amplitude was about 1% before installing FSTs, and the ripple amplitude reduced by ~1/2 due to FSTs. As shown in Fig. 3(a), the edge CTR rotation increases with increasing ripple loss power. Each arrow indicates the change in V_t in L-mode plasmas by installing FSTs under the condition of similar absorbed power (solid arrow: P_{ABS} ~ 1.4-1.8 MW, dotted arrow: P_{ABS} ~ 2.8-3 MW). Moreover, the profiles of the ion temperature (T_i) and the electron density (n_e) in the case with FSTs are similar to each profile in the case without FSTs in the peripheral region [14]. For example, the radial profiles of T_i and n_e in the case with P_{ABS} ~ 1.4-1.8 MW (solid arrows in Fig. 3(a)) are shown in Figs. 3(b) and 3(c). Therefore, it is thought that the difference in CTR rotation between the two discharges is not due to an increase in the pressure gradient at the edge, which can enhance the inward electric field. In other words, the effect of ripple loss and the pressure gradient on CTR-V_t is separately evaluated using data obtained with and without FST.

In order to confirm the location of the driving source of CTR rotation, beam perturbation techniques [14] are applied in an L-mode plasma. In this experiment, the plasma with low I_P (I_P = 0.87 MA, B_T = 3.8 T, q_{95} = 8.2) and large volume (*Vol.* = 72 m^3) was selected in order to enhance ripple losses. The large volume plasma suffers from the large ripple-induced loss in JT-60U. Off-axis PERP-NBs (see Fig. 2(b), absorbed power P_{ABS} ~ 2 MW/2 units) are injected with a square wave modulation at 2 Hz into the NBI-heated plasma. As mentioned above, the injection angle of PERP-NBs is 75 degrees with respect to the magnetic axis. For purely PERP-NB injections (i.e., with no external momentum input), one unit of CO PERP-NB and one unit of CTR PERP-NB are injected simultaneously. Figure 4(a) shows the waveforms of modulated V_t at r/a = 0.87 and 0.23 (solid lines), and the total NB power. Each trace is fitted to a sinusoidal function at the modulation frequency (dotted lines). The radial profiles of the phase delay of the modulated part of V_t (ϕ) and of the amplitude of the modulated part of V_t (V_{t0}) are shown in Figs. 4(b) and (c), respectively. The phase delay is considered from the start of NB injection. The profile of the prompt fast ion loss evaluated by the OFMC code [26] is also shown in Fig. 4(c). Large amplitude and small phase delay are recognized in the peripheral region ($0.7 < r/a < 0.9$), and this region agrees with the location at which fast ion losses take place. Therefore, we conclude that the fast ion losses due to the toroidal field ripple induce CTR toroidal rotation in the edge region.

3. Evaluation of Momentum Transport Coefficients and Intrinsic Rotation

In this section, the diffusive and non-diffusive terms of momentum transport, i.e., χ_ϕ and $V_{\rm conv}$ are separately evaluated using ϕ and V_{t0} profiles shown in Fig. 4(b) and (c), and V_t profiles driven by external torque input by NBs are calculated with χ_ϕ and $V_{\rm conv}$.

The toroidal momentum balance equations are written as

$$m_i \frac{\partial n_i V_t}{\partial t} = -\nabla \cdot M + S, \tag{1}$$

$$M = -m_i \chi_\phi \frac{\partial n_i V_t}{\partial r} + m_i V_{\rm conv} n_i V_t, \tag{2}$$

where m_i, n_i, M, and S are ion mass, ion density, toroidal momentum flux, and toroidal momentum source, respectively [18]. In this paper, ions are categorized as main (deuterium) and impurity ions, assuming that the toroidal rotation velocities of the main ions are the same as those of the carbon impurity ions, which are measured by charge exchange recombination spectroscopy (CXRS) [28]. We can express the modulated $n_i V_t$ assuming $n_i^c \tilde{V}_t >> \tilde{n}_i V_t^c$, where $\tilde{n}_i \tilde{V}_t$ is expressed as follows (the validity of this assumption in this experiment is shown later):

$$n_i^c \tilde{V}_t = n_i^c(r) V_{t0}(r) \sin(\omega t - \phi(r)), \tag{3}$$

where n_i^c and V_t^c are the time invariant terms of n_i and V_t, and $\tilde{n}_i$ and $\tilde{V}_t$ are the modulated parts of n_i and V_t, respectively. From equations (1)-(3), the time-independent solutions of χ_ϕ and $V_{\rm conv}$ can be obtained [18]. In order to apply this transient transport analysis method [14,18], strictly speaking, the data in the central region $0 < r/a < 0.2$ are needed, as shown by equations (9) and (10) in Ref. [18]. In the experimental condition discussed in this paper, the toroidal rotation velocity in this region was not measured because the neutral beam for the CXRS measurement is slightly off-axis. Therefore, we assumed a smooth fit to the profiles of $\phi(r)$ and V_{t0}(r) to cover this area. However, for the evaluations of χ_ϕ and $V_{\rm conv}$ in the region $0.3 < r/a < 0.65$, the errors due to this assumption are less than ±5%.

3.1 Toroidal rotation profile without external momentum source

Figures 5(a) and (b) show χ_ϕ and $V_{\rm conv}$ as evaluated from the above-mentioned modulation analysis (i.e., ϕ and V_{t0} profiles in Figs. 4(b) and (c)) assuming that the momentum source in the core region ($0.2 < r/a < 0.65$) is neg-

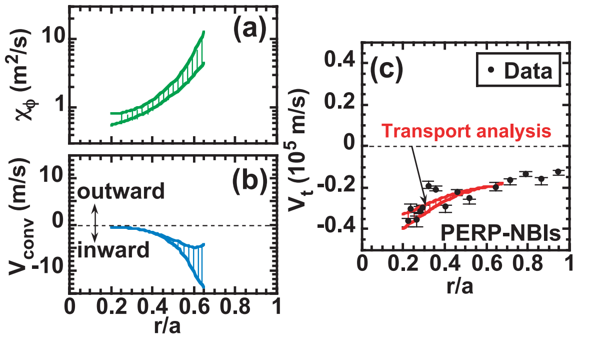

Fig. 5 Profiles of (a) toroidal momentum diffusivity (χ_ϕ) and (b) convection velocity ($V_{\rm conv}$) obtained from beam perturbation techniques shown in Fig. 4. (c) Experimental data (solid circles) in L-mode plasma with PERP-NBIs.

ligible (the momentum flux due to the modulated PERP-NBs, M, on the left-hand side of equation (2) is one order of magnitude smaller than $-m_i \chi_\phi \partial n_i V_t / \partial r$ and $m_i V_{\rm conv} n_i V_t$ at $r/a \sim 0.6$). The error bars shown in Figs. 5(a) and (b) mainly come from the fittings of V_{t0} and ϕ. These transport coefficients in the region $r/a > 0.7$ are not evaluated, because the driving source of CTR rotation is localized in this region, as shown in Fig. 4(c).

The measured V_t (solid circles) in the L-mode plasma ($I_P = 0.87$ MA, $B_T = 3.8$ T, $q_{95} = 8.2$) with PERP-NBIs is shown in Fig. 5(c), which is the same profile as in Fig. 1(b). The solid lines show V_t profiles evaluated from equations (1) and (2) using the derived momentum transport coefficients and the boundary condition at $r/a \sim 0.65$. As shown in Fig. 5(c), the measurement is almost reproduced by the calculation. This means that such CTR rotation with only PERP-NBs can be explained by momentum transport considering χ_ϕ and $V_{\rm conv}$. In this plasma, the amplitude of the modulated part of $\bar{n}_e$, which is also fitted to a sinusoidal function, is about 2% of the time invariant value [18]. If n_i changes (are modulated) 2% with the same phase as V_t, the modulated velocity part ($n_i^c \tilde{V}_t$) is about 5-10 times larger than the modulated density part ($\tilde{n}_i V_t^c$) in the region $0.2 < r/a < 0.7$. This means that the expression of equation (3) is suitable.

3.2 Toroidal rotation profile with external momentum source

We also treat the plasmas in which the external momentum source is injected, in order to investigate whether the toroidal rotation in the core region is determined by the momentum transport with the derived coefficients. The L-mode plasmas with low heating power, where the intrinsic rotation [19] is thought to be small, are selected for simple momentum transport study. In this study, the external torque and heating power of the base NB (see the schematic view of the time slice of NBI in Fig. 6(a)) are scanned. Experimental data (solid circles) in L-mode plasmas with one unit of CO tangential NB ($I_P = 1.2$ MA,

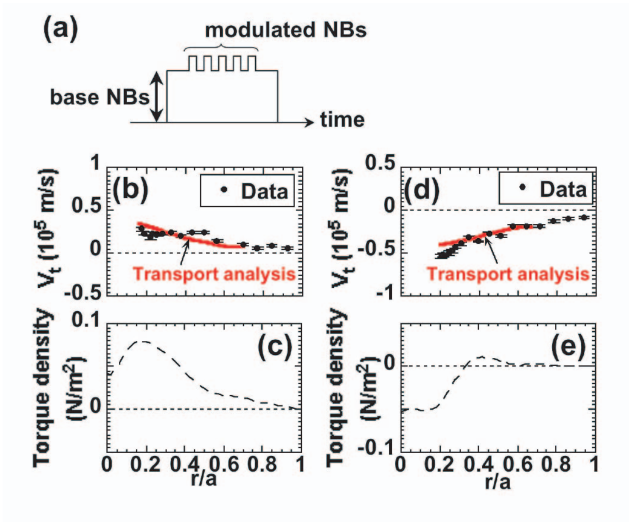

Fig. 6 (a) Schematic diagram of the time slice of NBI (base NBs + modulated NBs). Profiles of (b) V_t and (c) torque density with one unit of CO-NB (I_P = 1.2 MA, B_T = 3.8 T, q_{95} = 5.7, P_{ABS} = 2.7 MW, $\bar{n}_e = 1.2 \times 10^{19}$ m^{-3}), and (d) V_t and (e) torque density with one unit of CTR-NB (I_P = 0.87 MA, B_T = 3.8 T, q_{95} = 8.2, P_{ABS} = 2.1 MW, $\bar{n}_e = 1.6 \times 10^{19}$ m^{-3}). In both L-mode plasmas, one unit of PERP-NB is also injected for the CXRS measurements.

B_T = 3.8 T, normalized beta, β_N = 0.39, q_{95} = 5.7, P_{ABS} = 2.7 MW, and $\bar{n}_e = 1.2 \times 10^{19}$ m^{-3}) and one unit of CTR tangential NB (I_P = 0.87 MA, B_T = 3.8 T, β_N = 0.34, q_{95} = 8.2, P_{ABS} = 2.1 MW, and $\bar{n}_e = 1.6 \times 10^{19}$ m^{-3}) are shown in Figs. 6(a) and (d), respectively. In both plasmas, one unit of PERP-NB is injected for the CXRS measurements [28]. Toroidal momentum source (torque) density profiles of Figs. 6(b) and (d) are also shown in Figs. 6(c) and (e), respectively. The solid lines in Figs. 6(b) and (d) show V_t profiles evaluated by the above-mentioned equations (1) and (2), and χ_ϕ and V_{conv} derived in each discharge. In both the cases, the measured toroidal rotation profiles are almost reproduced by the calculations. This means that the steady-state toroidal rotation profiles in the presence and absence of external torque have been explained by the momentum transport in the core region of low β ($\beta_N \sim 0.4$) L-mode plasmas.

3.3 Intrinsic rotation

In higher β plasma, the V_t profiles cannot be explained with only the momentum transport model [19]. Figure 7(a) shows the radial profile of the measured V_t (solid circles) in the case with a higher heating power (P_{ABS} = 11 MW) L-mode plasma. The solid line in Fig. 7(a) shows the calculated V_t from the momentum transport equations using χ_ϕ and V_{conv} with the boundary condition (setting the measured V_t equal to the calculated one at $r/a \sim 0.65$). Although the measured V_t agrees with the calculation in the region $0.45 < r/a < 0.65$, the measured V_t deviates from the calculated one in the CTR-direction in the core

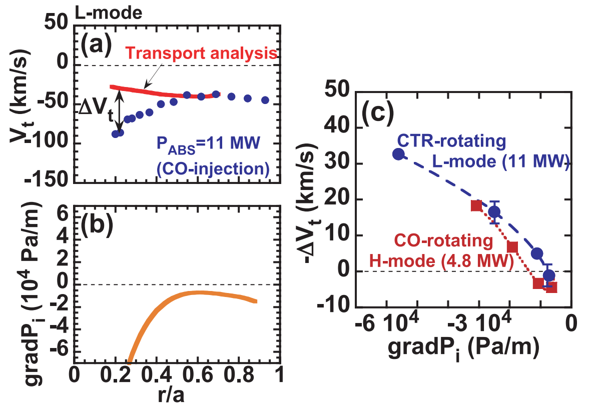

Fig. 7 (a) Profiles of measured (solid circles) and calculated (solid line) V_t, and (b) gradP$_i$ in the case of higher P_{ABS} (= 11 MW) L-mode plasma (I_p = 1.5 MA, B_T = 3.8 T). (c) $-\Delta V_t$ is plotted against gradP$_i$ for the CTR-rotating L-mode plasma (same discharge as in Figs. 7(a) and (b)) (solid circles), and for the co-rotation H-mode plasma (I_p = 1.2 MA, B_T = 2.7 T, P_{ABS} = 4.8 MW) (solid squares).

region $0.2 < r/a < 0.45$. In such plasmas, the large pressure gradient (gradP$_i$) is observed in the core region ($0.2 < r/a < 0.45$), as shown in Fig. 7(b). The difference between the measured V_t and the calculated one, i.e., $\Delta V_t = V_t(measurement) - V_t(calculation) = intrinsic\ rotation$, in the region $0.3 < r/a < 0.6$ is plotted against gradP$_i$ in Fig. 7(c) (solid circles). The symbols denote ΔV_t at r/a = 0.3, 0.4, 0.5, and 0.6. In these plasmas, the larger values of gradP$_i$ are obtained in the core region. As shown in Fig. 7(c), ΔV_t grows with increasing gradP$_i$. This tendency is almost the same, even in the CO-rotating H-mode plasmas (solid squares), over a wide range of χ_ϕ, which radially varies by about one order of magnitude ($\chi_\phi \sim$ 1-30 m^2/s). In this case, the local pressure gradient plays a role in determining the local value of intrinsic rotation velocity intrinsic rotation increases with increasing pressure gradient [19]. Proper evaluation of the momentum coefficients enables us to evaluate the intrinsic rotation.

4. Characteristics of χ_ϕ and V_{conv} in L- and H-mode Plasmas

Parameter dependences of the momentum transport coefficients (i.e., χ_ϕ and V_{conv}) on heating power and I_p are shown in this section. The profiles of χ_ϕ and V_{conv} during the heating power scan for L-mode plasmas are shown in Figs. 8(a) and (b), respectively. The absorbed power range varied over 2.4 MW < P_{ABS} < 10.7 MW under otherwise similar conditions. Over the entire power range, the L-mode phase was maintained due to the high power threshold at the high B_T (= 3.8 T). Other plasma parameters for this series of discharges were I_p = 1.5 MA, q_{95} = 4.2, $\bar{n}_e$ = 1.6-2.3 $\times 10^{19}$ m^{-3}, and *Vol.* = 74 m^3. These plasmas are the typical L-mode plasmas that satisfy the L-mode scaling law of stored energy [29]. Even in the L-

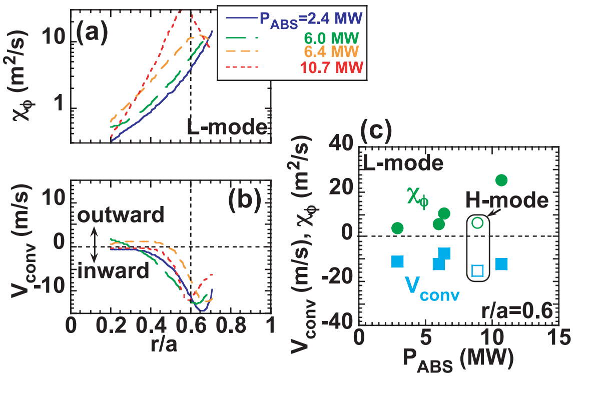

Fig. 8 Profiles of (a) χ_ϕ and (b) V_{conv} during a heating power scan in L-mode plasmas (I_P = 1.5 MA, B_T = 3.8 T, q_{95} = 4.2, 2.4 MW < P_{ABS} < 10.7 MW, *Vol.* = 74 m^3, $\bar{n}_e$ = 1.6-2.3 × 10^{19} m^{-3}). (c) Dependence of χ_ϕ and V_{conv} on absorbed power at r/a = 0.6. The data in the H-mode phase is also plotted with open circles and squares.

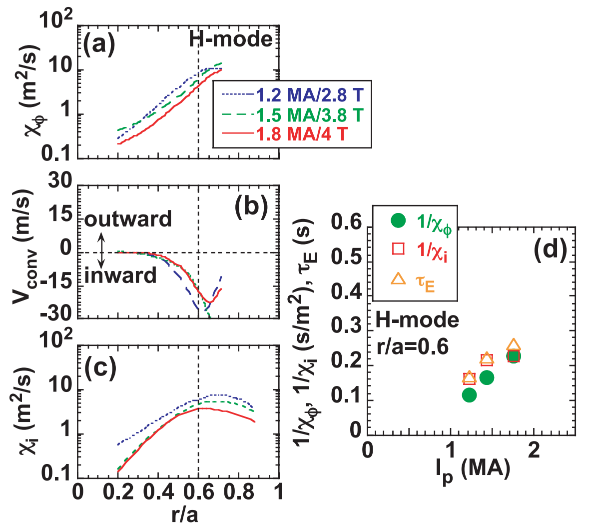

Fig. 9 Profiles of (a) χ_ϕ, (b) V_{conv}, and (c) χ_i during an I_p scan in H-mode plasmas (I_p/B_T = 1.2/2.8, 1.5/3.8, 1.8/4 MA/T, q_{95} = 4.3-5.1, P_{ABS} = 7.2-8.9 MW, *Vol.* = 73-77 m^3, $\bar{n}_e$ = 2.0-2.5 × 10^{19} m^{-3}). (c) Dependence of $1/\chi_\phi$ and $1/\chi_i$ (at r/a = 0.6) and τ_E on I_p.

mode regime, these plasmas stay in a low-collisionality and small-Larmor radius regime with ρ^*_{pol} = 0.03-0.05 and ν^* = 0.07-0.14. Here, ρ^*_{pol} is the ion poloidal Larmor radius normalized to the minor radius, and ν^* is the effective electron collision frequency normalized to the bounce frequency. The normalized beta varies from 0.39 to 1. The momentum diffusivity χ_ϕ increases systematically with increasing heating power over the whole radius. Non-diffusive inward flux exists and has a maximum value at r/a ~ 0.6. The dependences of χ_ϕ and V_{conv} at r/a = 0.6 on absorbed power are shown in Fig. 8(c). The momentum diffusivity at r/a = 0.6 roughly scaled linearly with heating power in this data set. The data in the H-mode phase is also plotted in Fig. 8(c). The momentum diffusivity in the H-mode is smaller than in the L-mode by a factor of 2 to 3.

We also investigate the dependences of χ_ϕ and V_{conv} on I_p in H-mode plasmas. Figures 9(a)-(c) illustrate the radial profiles of χ_ϕ, V_{conv}, and χ_i in an I_p scan, where B_T also varies so that q_{95} has a similar value (I_p/B_T = 1.2/2.8, 1.5/3.8, 1.8/4 MA/T). For these plasmas, two units of CO tangential NB, a half unit of CTR tangential NB and two to three units of PERP-NBs are injected with P_{ABS} = 7.2-8.9 MW. Other plasma parameters for this series of discharges were *Vol.* = 73-77 m^3 and $\bar{n}_e$ = 2.0-2.5 × 10^{19} m^{-3} (β_N = 0.9-1.4, ρ^*_{pol} = 0.05-0.06, and ν^* = 0.04-0.05). The momentum diffusivity χ_ϕ decreases with increasing I_p over the whole radius. Also, V_{conv} and χ_i decrease with increasing I_p. The dependences of $1/\chi_\phi$ and $1/\chi_i$ at r/a = 0.6 and the energy confinement time τ_E on I_p are also shown in Fig. 9(d). These parameters are almost proportional to I_p, and the coefficients have similar values ($1/\chi_\phi$ ~ 0.12I_p, $1/\chi_i$ ~ 0.14 I_p, τ_E ~ 0.15 I_p). This observation suggests that momentum transport has a relationship with thermal ion heat transport. A more detailed discussion of the relationship is presented in the next section.

5. Relationships Among Transport Coefficients, χ_ϕ, and χ_i and V_{conv}

In this section, the relationships among χ_ϕ, χ_i, and V_{conv} in H-mode plasmas are resolved using I_p and P_{ABS} scans. In this study, the relationship between χ_ϕ and χ_i is found for the first time after separating the diffusive and convective terms. The comparison of χ_ϕ and χ_i for each I_p (1.2, 1.5, and 1.8 MA) in the region 0.25 < r/a < 0.6 is shown in Fig. 10(a). These traces come from the profiles shown in Figs. 9(a) and (c), and the smaller values of χ_ϕ correspond to those in the inner region. One can see that χ_ϕ increases with increasing χ_i and χ_ϕ/χ_i ~ 1. This tendency is observed over a wide range of radii for each discharge. A similar data set during the heating power scan (4.8 MW < P_{ABS} < 10 MW) is shown in Fig. 10(b), where two units of CO tangential NBs and PERP-NBs are injected. Other plasma parameters for this series of discharges were I_p = 1.2 MA, B_T = 2.8 T, q_{95} ~ 4.4, *Vol.* ~ 67 m^3, and $\bar{n}_e$ = 1.8-2.2 × 10^{19} m^{-3} (β_N = 1.1-1.8, ρ^*_{pol} = 0.06-0.07, and ν^* = 0.07-0.09). In this P_{ABS} scan, χ_ϕ/χ_i ~ 1-3. The reasons for the difference in χ_ϕ/χ_i between the two scans (Figs. 10(a) and (b)), where the plasma volume and torque input are different, have not been identified. Thus, a further investigation of the parameter dependence of χ_ϕ/χ_i is an important issue. In the case of the conventional steady-state analyses without considering the convective term, the evaluated χ_ϕ tended to be much smaller than χ_i [12]. However, our results from the transient momentum transport analysis suggest that χ_ϕ is close to χ_i. This means that the momentum diffusivity is also anomalous to a similar level as the heat diffusivity.

The correlation between V_{conv} and χ_ϕ is also found for

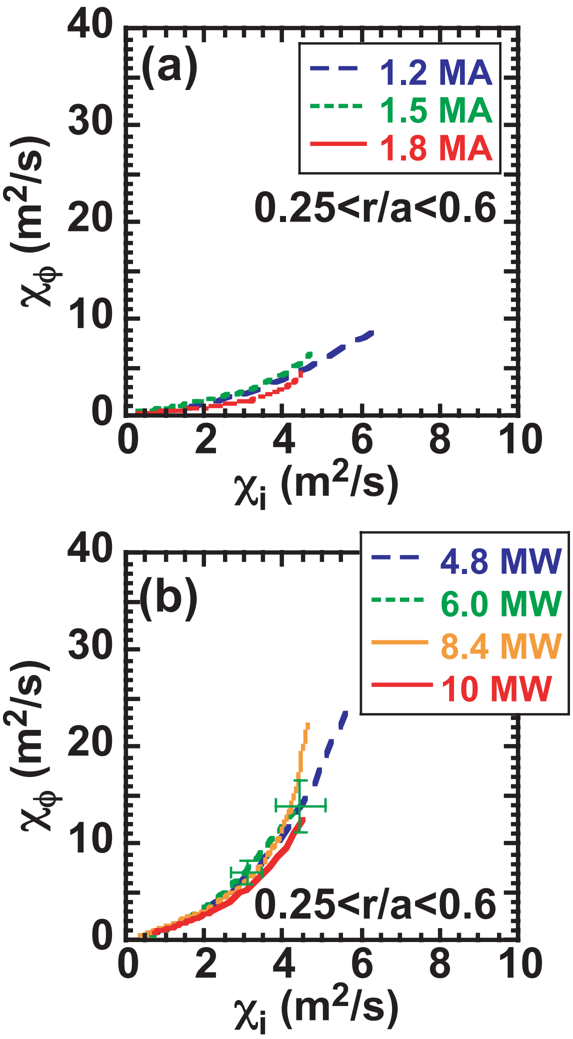

Fig. 10 Relationship between χ_ϕ and χ_i (a) during the I_p scan (same discharges as in Fig. 9), and (b) during the heating power scan (I_p = 1.2 MA, B_T = 2.8 T, $q_{95} \sim 4.4$, 4.8 MW < P_{ABS} < 10 MW, *Vol.* ~ 67 m^3, $\bar{n}_e$ = 1.8-2.2 × 10^{19} m^{-3}) in H-mode plasmas. Each trace comes from the profiles in the region 0.25 < r/a < 0.6.

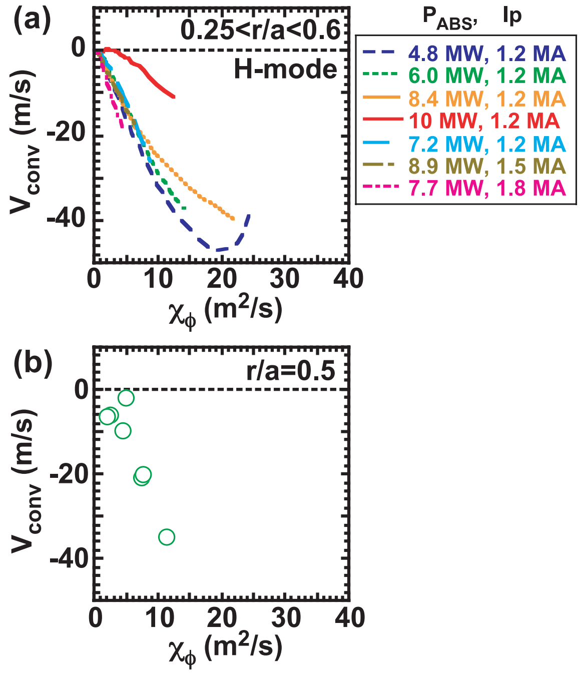

Fig. 11 Correlation between V_{conv} and χ_ϕ (a) from the profile data for each discharge, and (b) at r/a = 0.5 in H-mode plasmas. The data set given in Fig. 10 is used.

the first time. Figure 11(a) shows the correlation between $-V_{conv}$ and χ_ϕ in the region 0.25 < r/a < 0.6 for each discharge. The same data set shown in Fig. 10 is used; therefore, the smaller values of χ_ϕ correspond to those in the inner region. In addition, the correlation for fixed radius (r/a = 0.5) is shown in Fig. 11(b). The inward convection velocity ($-V_{conv}$) increases with increasing χ_ϕ over a wide range of radii for each discharge and also at the fixed radius r/a = 0.5 in P_{ABS} and I_p scans. The value of V_{conv}/χ_ϕ is around −2.5 to −0.7 m^{-1} in this data set. The parameter dependence of V_{conv}/χ_ϕ is an important area for future study; however, this finding of the correlation between χ_ϕ and V_{conv} can contribute to the understanding of the anomalous momentum transport (for example, see Ref. [24]).

6. Summary

The elements determining the toroidal rotation V_t profile have been identified, and the roles of these elements on the V_t profile are also found. The fast ion losses due to the toroidal field ripple induce CTR rotation in the edge region. As a new momentum source, this edge-localized momentum source has been used for transient momentum transport analysis. χ_ϕ and V_{conv} have been separately evaluated using transient momentum transport analysis, and these properties are investigated for L- and H-mode plasmas. χ_ϕ increases with increasing heating power, and decreases with increasing I_p. We have found that χ_ϕ, when separated from the convective term, increases with increasing χ_i ($\chi_\phi/\chi_i \sim$ 1-3). $-V_{conv}$ increases with increasing χ_ϕ ($V_{conv}/\chi_\phi \sim$ −2.5 to −0.7 m^{-1}) in the region 0.25 < r/a < 0.6. These tendencies are similar over the entire ranges of heating power (4.8 MW < P_{ABS} < 10 MW) and plasma current (1.2 MA < I_p < 1.8 MA). At low β (β_N < 0.4) or heating power, the steady-state V_t profiles in CO-, CTR-, and PERP-NB injected plasmas can be almost reproduced by calculations with χ_ϕ or V_{conv}, respectively. At higher β, the CTR-directed intrinsic rotation increases with increasing local pressure gradient.

Acknowledgments

This study was partly supported by JSPS, Grant-in-Aid for Young Scientists (B) No 17740374. The authors acknowledge the members of the Japan Atomic Energy Agency who have contributed to the JT-60U projects.

[1] Y. Kamada, Plasma Phys. Control. Fusion **42**, A65 (2000).
[2] Special issue on Progress in the ITER Physics Basis [Nucl. Fusion **47**, S18 (2007)].
[3] D.J. Ward *et al.*, Phys. Plasmas **2**, 1570 (1995).
[4] M. Takechi *et al.,* Phys. Rev. Lett. **98**, 055002 (2007).
[5] H. Reimerdes *et al.*, Phys. Rev. Lett. **98**, 055001 (2007).
[6] E.J. Synakowski *et al.*, Nucl. Fusion **39**, 1733 (1999).
[7] Y. Sakamoto *et al.*, Nucl. Fusion **41**, 865 (2001).
[8] T. Luce *et al.*, in *Proceedings of the 21st IAEA Fusion Energy Conference, Chengdu, 2006* (IAEA, China, 2006) PD3.
[9] J. Kim *et al.*, Phys. Rev. Lett. **72**, 2199 (1994).
[10] K. Nagashima *et al.*, Nucl. Fusion **34**, 449 (1994).
[11] K. Ida *et al.*, J. Phys. Soc. Jap. **67**, 4089 (1998).
[12] ITER Physics Expert Group on Confinement and Transport, ITER Physics Expert Group on Confinement Modeling and Database and ITER Physics Basis Editors, Nucl. Fusion **39**, 2175 (1999).
[13] W.D. Lee *et al.*, Phys. Rev. Lett. **91**, 205003 (2003).
[14] M. Yoshida *et al.*, Plasma Phys. Control. Fusion **48**, 1673 (2006).
[15] A. Bortolon *et al.*, Phys. Rev. Lett. **97**, 235003 (2006).
[16] T. Tala *et al.*, Nucl. Fusion **47**, 1012 (2007).
[17] J. E. Rice *et al.*, Nucl. Fusion **47**, 1618 (2007).
[18] M. Yoshida *et al.*, Nucl. Fusion **47**, 856 (2007).
[19] M. Yoshida *et al.*, Phys. Rev. Lett. in press.
[20] T. Tala *et al.*, Plasma Phys. Control. Fusion **49**, B291 (2007).
[21] Y.B. Kim, P.H. Diamond and R.J. Groebner, Phys. Fluids B **3**, 2050 (1991).
[22] B. Coppi, Nucl. Fusion **42**, 1 (2002).
[23] O.D. Gurcan, P.H. Diamond, T.S. Hahm, *et al.*, Phys. Plasmas **14**, 042306 (2007).
[24] T.S Hahm, P.H. Diamond, O.D Gurcan and G. Rewoldt, Phys. Plasmas **14**, 072302 (2007).
[25] A.G. Peeters, C. Angioni and D. Strintzi, Phys. Rev. Lett. **98**, 265003 (2007).
[26] K. Shinohara *et al.*, Nucl. Fusion **47**, 997 (2007).
[27] H. Takenaga and the JT-60 Team, Nucl. Fusion **47**, S563 (2007).
[28] Y. Koide *et al.*, Rev. Sci. Instrum. **72**, 119 (2001).
[29] H. Shirai *et al.*, in Plasma Physics and Controlled Nuclear Fusion Research 1994 (*Proc. 15th Int. Conf. Seville, 1994*), Vol. 1, p. 355, IAEA, Vienna (1995).